

Investigation of sound sources in subsonic jets using causality methods on LES data

Christophe Bogey* and Christophe Bailly†

Laboratoire de Mécanique des Fluides et d'Acoustique

UMR CNRS 5509, Ecole Centrale de Lyon

69134 Ecully, France

Noise sources are investigated in subsonic jets at Mach numbers $M = 0.6$ and $M = 0.9$, with Reynolds numbers $Re_D = 1700$ and $Re_D \geq 10^5$, using data provided by Large Eddy Simulations (LES). The cross-correlations between signals of the radiated sound pressure and turbulence signals along jet axis and shear layer are in particular calculated. The normalized correlations are found to be significant, around 0.10, between the pressure radiated in the downstream direction and the centerline flow quantities. In the cases involving the sideline pressure or flow quantities along the shear layer, the correlations are much smaller. The maximum correlations are observed on the jet axis just at the end of the potential core, and fall at large emission angles. Furthermore the correlations appear to be lower as the Mach number is reduced, and to be enhanced as the Reynolds number is decreased. These correlations can be expected to be mostly due to the noise source radiating downstream, which may thus be located on the jet centerline at the end of the potential core. This flow region is moreover characterized by a dominant frequency over a large axial distance and by a high level of intermittency.

I. Introduction

More than fifty years after Lighthill's pioneering work in 1952, noise generation mechanisms in subsonic jets are still not well-established in the literature.¹ This matter is to a great extent due to the fact that jet noise theories are closely dependent on the understanding of turbulence, which has significantly evolved. In the fifties, turbulence was for instance regarded only as fine-grained turbulence, whereas it was considered to be strongly dominated by coherent structures in the seventies and the eighties. There are also difficulties in identifying sound sources directly from the radiated sound field. The knowledge of the radiated acoustic field allows however to shed light on the sound source region. The jet-noise-source strength distribution can in particular be obtained using directional-microphone techniques based on ray-tracing. Chu & Kaplan² thus shown that the dominant sound source region in high-subsonic jets is located just downstream of the potential core. The variations of noise properties with jet velocity and emission angle can also bring support to the different jet noise theories. Lush³ for example compared his measurements for subsonic jets with the predictions of Lighthill's theory, in order to discuss the validity of the convective amplification factor resulting from the theory, see also the review of Goldstein.⁴ The trends exhibited by the experimental data at different emission angles moreover suggest clearly that jet noise is made of two basic components:⁵⁻⁷ one dominating in the downstream direction, another dominating in the sideline direction. The variations of jet noise with the Reynolds number⁸ are also particularly relevant to characterize the sound sources. Crighton⁹ for instance noticed that the noise radiated by excited jets changes below the Reynolds number $Re_D = u_j D / \nu \simeq 10^5$ (u_j is the jet velocity, c_0 is the speed of sound in the ambient medium, and ν is the kinematic molecular viscosity). As the Reynolds number decreases, simulation results obtained by the authors of the present paper further shown that the downstream noise component is not appreciably modified, whereas the sideline noise tends to disappear.¹⁰ To study jet noise sources from the sound field alone, we can finally note that an accurate

*CNRS research scientist, christophe.bogey@ec-lyon.fr

†Professor at Ecole Centrale de Lyon, AIAA Member, christophe.bailly@ec-lyon.fr

description of the near pressure field may be especially appropriate.^{11,12} Sound source locations in terms of the turbulence maxima were discussed in this way by Zaman¹¹ for a jet at Mach number $M = u_j/c_0 = 0.5$.

To investigate jet noise generation mechanisms, another approach consists in searching for direct connections between the flow field and the radiated sound field. Specific events generating noise can first be tracked from simultaneous visualizations of the two fields. Pairing and tearing of vortical structures in the shear layer could have thus been linked to isolated acoustic waves radiated by the jets.^{13,14} More interestingly, the quasi-periodic intrusion of vortical structures into the jet at the end of the potential core has been connected to the noise component radiated in the downstream direction.¹⁴ Jet noise sources can be also identified directly by using the causality method, in which cross-correlations between various flow quantities inside the jet and the radiated sound pressure are calculated. In the seventies, Siddon & Rackl¹⁵ and Hurd *et al.*¹⁶ selected for instance the incompressible pressure fluctuations as the flow quantity. Hurd *et al.*¹⁶ made in particular measurements on a jet engine, with a pressure probe located one diameter off the jet axis at the end of the potential core. For a jet at $M = 0.85$, they observed normalized correlations of 0.139 with the acoustic pressure at an angle of 20° to the jet axis, down to 0.006 at 90° to the jet axis. The correlation levels were also found to decrease dramatically as the Mach number decreases, as illustrated by the correlation of 0.025 obtained at 20° to the jet axis for a jet at $M = 0.52$. Other authors¹⁷⁻²² determined the cross-correlations between the velocity fluctuations inside the jet and the radiated pressure. The correlations measured for jets¹⁷⁻²¹ with Mach numbers in the range $0.3 \leq M \leq 0.4$ are however quite weak. At 40° to the jet axis, Lee & Ribner¹⁷ obtained for instance a maximum broadband correlation of only 0.02 for a $M = 0.3$ jet, while Seiner¹⁸ noted that the correlations at 90° to the jet axis for a $M = 0.33$ jet are too small to be accurately evaluated. In this case, filtering the flow and acoustic components^{17,18} or using conditional sampling^{19,20} was necessary to enhance the amplitude of the correlations. The correlations thus obtained from pressure radiated at small angles from the jet axis have allowed to show the source-strength distribution along the jet axis, and to discuss the contributions of the so-called shear-noise and self-noise. The region generating noise at the dominant frequency is in particular found after the end of the potential core. The correlations reported by Schaffar²² for a jet at $M = 0.98$ exhibited higher levels than those at $M \simeq 0.3$ mentioned above. Schaffar²² indeed observed maximum broadband correlations with pressure at 30° to the jet axis of about 0.06 for points on the jet axis just downstream of the jet core. More recently, Panda *et al.*^{23,24} measured cross-correlations between the radiated pressure and flow quantities such as density and velocity fluctuations, for jets at Mach numbers 0.95 and 1.8. They observed higher correlation levels at $M = 1.8$, and shown the sharp fall of the maximum correlation with the radiation angle. Furthermore, the correlations between flow quantities along the shear layer and pressure at 30° to the jet axis were found to be significant at $M = 1.8$, but very weak at $M = 0.95$.

In the present work, noise sources in subsonic jets are investigated using the causality method for jets at Mach numbers $M = 0.6$ and $M = 0.9$, with Reynolds numbers $Re_D = 1700$ and $Re_D \geq 10^5$, computed by Large Eddy Simulation (LES). Cross-correlations are calculated between the broadband turbulence signals and the broadband sound pressure signals provided by LES. This work is the continuation of earlier studies where different subsonic jets were simulated. The simulations were performed using a solver developed for direct noise computations with low-dissipative and low-dispersive numerical schemes.²⁵ The LES approach followed was based on an explicit selective filtering for subgrid modeling,^{26,27} in order to preserve the effective Re_D given by the jet initial conditions. A jet at $M = 0.9$ and $Re_D = 4 \times 10^5$ was first considered. Flow and sound properties in agreement with high-Reynolds-number experimental data were obtained,²⁶ and the influence of the inflow conditions²⁸ and of the subgrid modeling²⁹ on results was shown. The effects of the Mach and Reynolds numbers on the noise radiated by jets at Mach numbers 0.6 and 0.9, with Reynolds numbers varying from 1700 up to 4×10^5 , were then described,¹⁰ in order to characterize the two subsonic jet noise components. Two sound sources were exhibited: a Reynolds number-dependent source, predominant for large radiation angles, connected to the randomly-developing turbulence, and a deterministic source, radiating downstream. In the present work, we focus on the jets at $M = 0.6$ and $M = 0.9$, with Reynolds numbers $Re_D = 1700$ and $Re_D \geq 10^5$. The aim is in particular to study the influence of the Mach and Reynolds numbers on the flow-noise cross-correlations. The correlations considered are those between the radiated pressure, and the fluctuating velocities, the Reynolds stresses, the turbulent kinetic energy and the vorticity norm along the jet axis and the shear layer. Attention is specially drawn to the pressure obtained at the radiation angles, relative to an origin at the end of the potential core, of 40° and 90° from the jet direction. Finally note that the centerline turbulence at the end of the jet core, where the maximum correlations with the radiated noise are likely to be found, is also briefly examined.

The paper is organized as follows. In section II, the main features of the numerical procedure are presented the parameters of different simulations are given, and the observation points are defined. The cross-correlations between the jet flow quantities and the radiated pressure are shown in section III, where properties of the centerline turbulence at the end of the jet core are also reported. Finally, section IV contains concluding remarks.

II. Simulation parameters

A. Numerical procedure

The numerical algorithm and parameters are those of the simulation²⁶ of a Mach $M = 0.9$, Reynolds $Re_D = 4 \times 10^5$ jet, referred to as LESac or LESsf in earlier papers.^{26, 28, 29} The simulation time is however doubled for an accurate evaluation of the flow-noise cross-correlations.

The Cartesian filtered compressible Navier-Stokes equations are solved using numerical schemes with low dispersion and low dissipation properties.²⁵ A thirteen-point finite-difference scheme is used for spatial discretization, and an explicit six-stage Runge-Kutta algorithm is applied for time integration. Grid-to-grid oscillations are removed thanks to an explicit filtering which is optimized to damp only the short waves discretized by less than four points per wavelength. It is used to ensure numerical stability, and also to take into account the effects of the subgrid energy-dissipating scales without affecting the resolved scales. This approach was developed to preserve the effective Reynolds number of the jet, which might not be possible using eddy-viscosity subgrid models such as the dynamical Smagorinsky model.²⁹ Furthermore, in order to compute the radiated noise directly, non-reflective boundary conditions are implemented, with the addition of a sponge zone in the jet at the outflow.³⁰

The computational domain is discretized by a 12.5 million point Cartesian grid with 15 points within the range $0 \leq r \leq r_0$, and extends radially up to $r = 15r_0$ from the jet axis. Due to stretching of the axial mesh size for $x \geq 26r_0$, the turbulent flow is computed accurately up to a distance of $x = 25r_0$, and the sound field is resolved for Strouhal numbers $St = fD/u_j < 2$ up to $x = 30r_0$. The simulation times T are doubled with respect to the earlier studies^{10, 26} in order to make sure of the convergence of the cross-correlations. The corresponding Strouhal number is now $D/(Tu_j) = 4.9 \times 10^{-4}$. The statistics obtained from the time period T are for instance found not to differ appreciably from those obtained from the time period $2T/3$. Spectra and cross-correlations are performed from velocity and pressure signals of total time T_s such as $D/(T_s u_j) = 5.2 \times 10^{-4}$ in term of minimal Strouhal number. In addition, the pressure signals are filtered using moving averaging in order to remove the low-frequency components with $St < 0.05$.

B. Definition of the simulations

Four isothermal round jets are considered. Their initial conditions are identical except for the diameter and the jet exit velocity, yielding Mach numbers of 0.6 and 0.9 and Reynolds numbers $Re_D = 1700$ and $Re_D \geq 10^5$, as presented in table 1. The LESm09hre simulation is the jet simulation at Mach $M = 0.9$ and at the high Reynolds number $Re_D = 4 \times 10^5$ also referred to as LESac^{26, 28} or as LESsf²⁹ in earlier papers. In the LESm09re1700 simulation, the Mach number of 0.9 is maintained but the Reynolds number is decreased down to $Re_D = 1700$. In the LESm06hre and LESm06re1700 simulations, the Mach number is reduced down to $M = 0.6$. The former simulation is at a high Reynolds number $Re_D \geq 10^5$, whereas the latter is at the low Reynolds number $Re_D = 1700$ as in LESm09re1700.

Table 1. Mach and Reynolds numbers of the simulated jets, and location of the end of the potential core x_c and of the observation points M_{40} and M_{90} .

	M	Re_D	x_c	$M_{40}(x, y)$	$M_{90}(x, y)$
LESm09hre	0.9	4×10^5	$10.2r_0$	$(28r_0, 15r_0)$	$(10r_0, 15r_0)$
LESm09re1700	0.9	1.7×10^3	$15.8r_0$	$(29r_0, 11r_0)$	$(16r_0, 15r_0)$
LESm06hre	0.6	2.7×10^5	$9.5r_0$	$(27r_0, 15r_0)$	$(10r_0, 15r_0)$
LESm06re1700	0.6	1.7×10^3	$13.3r_0$	$(29r_0, 13r_0)$	$(13r_0, 15r_0)$

In all the simulations, the inflow parameters (shear-layer thickness, forcing) are identical. They are those

specified for the LESm09hre simulation.^{26,28} Mean profiles of velocities, pressure and density are imposed at the jet inflow boundary. The axial velocity is given by a hyperbolic-tangent profile describing an annular shear layer of radius r_0 and of momentum thickness δ_θ , with a ratio $\delta_\theta/r_0 = 0.05$. Radial and azimuthal velocities are set to zero, pressure is set to the ambient pressure, and the mean density profile is obtained using a Crocco-Busemann relation for an isothermal jet.²⁶ To trip the turbulent transition, small random disturbances are added to the velocity profiles in the shear layer zone. Finally note that the influence of the inflow conditions and forcing on the jet flow and sound fields was recently studied.²⁸

C. Definition of the observation points

Snapshots of the pressure fields generated by the jets were presented in a previous paper.¹⁰ The properties of the sound radiated in the downstream and sideline directions were also described in detail. Two noise components were thus characterized. The first component appears as a well-marked peak at a low Strouhal number in the spectra obtained in the jet direction. In the present jets, it was found to dominate at about 30° to the jet axis, with Strouhal peaks of $St \simeq 0.3$ at high Reynolds number, and of $St \simeq 0.2$ at $Re_D = 1700$. The second component was observed to be predominant for large radiation angles. It is broadband and strongly dependent on the Reynolds number.

To study noise sources in the jets via the causality method, pressure and velocity are recorded at the observations points represented in the snapshot of figure 1. The pressure signals are obtained along the lines defined by $y = 15r_0$ and $z = 0$, and by $x = 29r_0$ and $z = 0$. The turbulence signals are provided along the jet axis at $y = z = 0$ and along the shear layer at $y = r_0$ and $z = 0$.

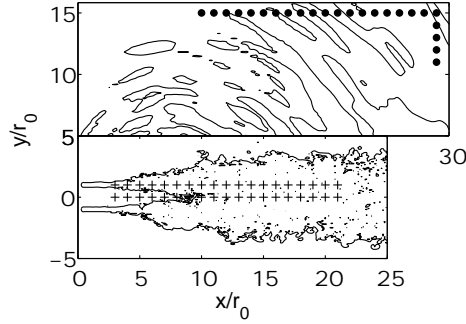


Figure 1. Visualization of the observation points: • in the acoustic field, + in the jet flow. Representation in the plane $z = 0$ of the vorticity contour $|\omega| = 1.2 \times 10^4 \text{ s}^{-1}$, and of the pressure contours $p' = [-60, 60] \text{ Pa}$ for the simulation LESm09hre.

The turbulence quantities measured in the jet flow are the fluctuating velocities u' , v' and w' , the Reynolds stresses u'^2 , v'^2 , and w'^2 , the turbulent kinetic energy $k = (u'^2 + v'^2 + w'^2)/2$ and the vorticity norm $|\omega|$. These quantities are correlated with the radiated fluctuating pressure p' to determine the cross-correlation functions C_{up} , C_{vp} , C_{wp} , C_{uup} , C_{vvp} , C_{wvp} , $C_{k p}$, and $C|\omega|p$. The normalized cross-correlations between the flow quantities u' , v' , k , and $|\omega|$ at point \mathbf{x}_1 and pressure at point \mathbf{x}_2 are for instance calculated in the following way:

$$\left\{ \begin{array}{l} C_{up}(\mathbf{x}_1, \mathbf{x}_2, t) = \frac{\langle u'(\mathbf{x}_1, T) p'(\mathbf{x}_2, T+t) \rangle}{\langle u'^2(\mathbf{x}_1, T) \rangle^{1/2} \langle p'^2(\mathbf{x}_2, T) \rangle^{1/2}} \\ C_{uup}(\mathbf{x}_1, \mathbf{x}_2, t) = \frac{\langle u'^2(\mathbf{x}_1, T) p'(\mathbf{x}_2, T+t) \rangle}{\langle u'^4(\mathbf{x}_1, T) \rangle^{1/2} \langle p'^2(\mathbf{x}_2, T) \rangle^{1/2}} \\ C_{k p}(\mathbf{x}_1, \mathbf{x}_2, t) = \frac{\langle k(\mathbf{x}_1, T) p'(\mathbf{x}_2, T+t) \rangle}{\langle k^2(\mathbf{x}_1, T) \rangle^{1/2} \langle p'^2(\mathbf{x}_2, T) \rangle^{1/2}} \\ C|\omega|p(\mathbf{x}_1, \mathbf{x}_2, t) = \frac{\langle |\omega|(\mathbf{x}_1, T) p'(\mathbf{x}_2, T+t) \rangle}{\langle |\omega|^2(\mathbf{x}_1, T) \rangle^{1/2} \langle p'^2(\mathbf{x}_2, T) \rangle^{1/2}} \end{array} \right.$$

where $\langle \cdot \rangle$ denotes time averaging and t is the time delay between the turbulence and the pressure signals.

In the present simulated jets, the potential core length is not constant due to Mach and Reynolds number effects. The location of the end of the potential core x_c , determined from the centerline mean axial velocity u_c

using $u_c(x_c) = 0.95u_j$, varies from $x_c = 9.5r_0$ up to $x_c = 15.8r_0$, as shown in table 1. To obtain results at fixed radiation angles, two points M_{40} and M_{90} defining angles of 40° and 90° from the jet axis, relative to an origin at the end of the jet core, are therefore selected among the observation points in the acoustic field. Their locations are given in table 1 for the different simulations.

In the next section, four cases will then be investigated, depending on whether correlations are calculated between pressure at the point M_{40} or M_{90} , and turbulence along the jet axis or along the shear layer. They are represented in figure 2, and referred to as M_{40}/axis , $M_{40}/\text{shear-layer}$, $M_{90}/\text{shear-layer}$ and M_{90}/axis . Another case will be also considered to study the angular dependence of the results, by correlating the centerline turbulence at $x = x_c$ with the pressure at the different observation points in the acoustic field.

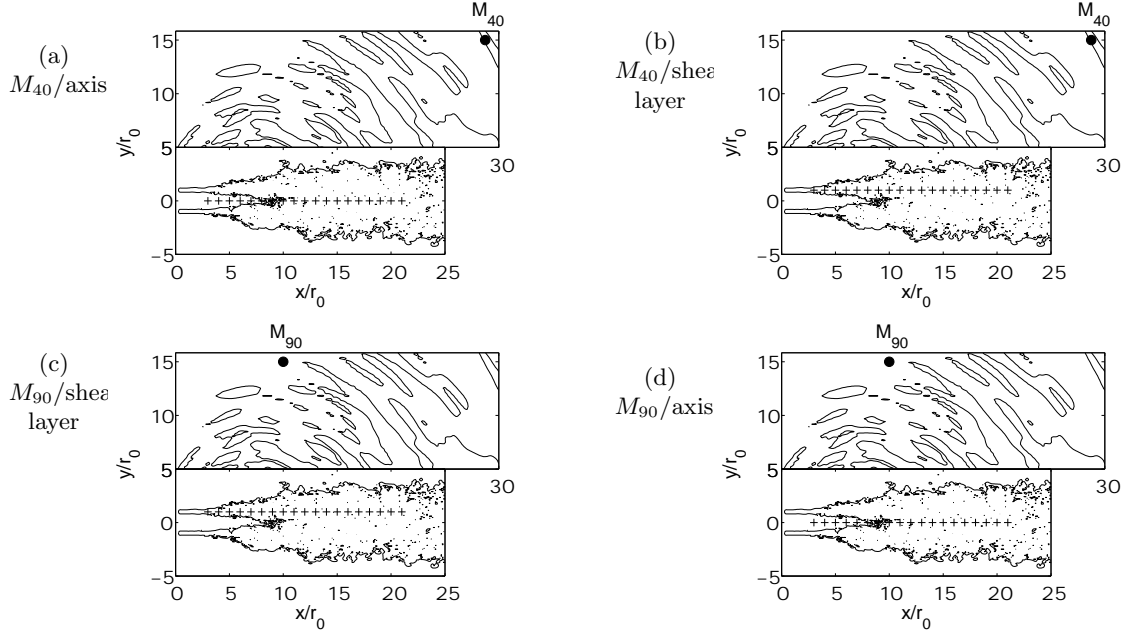


Figure 2. Sketch of the four cases in which cross-correlations are calculated between pressure at the point M_{40} or M_{90} , and flow quantities along the jet axis ($y = 0$) or along the shear layer ($y = r_0$).

The properties of the sound fields at the points M_{40} and M_{90} for which pressure will be correlated with the jet turbulence are now checked. The spectra obtained at point M_{40} at the radiation angle of 40° are shown in figure 3(a) for the $M = 0.9$ jets and in figure 3(b) for the $M = 0.6$ jets. At $M = 0.9$, the spectra are clearly dominated by frequency peaks typical of the downstream noise component. At $M = 0.6$, the downstream component peak is also apparent at the low Reynolds number. However at the high Reynolds number, the contributions of the two jet noise components cannot be distinguished.

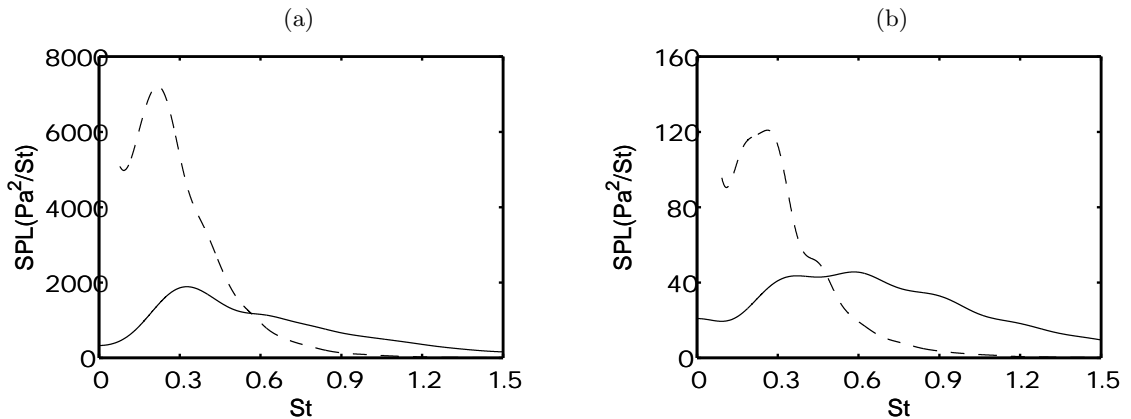


Figure 3. Pressure spectra obtained at the point M_{40} as a function of Strouhal number $St = fD/u_j$: (a) Mach 0.9 jets, (b) Mach 0.6 jets; at: ——— high Reynolds number, - - - $Re_D = 1700$.

The pressure spectra obtained at point M_{90} in the sideline direction are presented in figures 4(a) and 4(b) for the jets at Mach 0.9 and 0.6. These spectra correspond to those reported in a previous paper.¹⁰ Their characteristics were shown to be those of the broadband noise component attributed to the randomly-developing turbulence, at high Reynolds number but also at $Re_D = 1700$. Note that at a given Reynolds number, the shapes of the spectra obtained for the jets at $M = 0.9$ and $M = 0.6$ are very similar. The dramatic influence of the Reynolds number on the sideline spectra is also observed. As the Reynolds number decreases, a significant part of the high-frequency noise disappears. Consequently, the peak frequency is lower, down to a Strouhal number $St \simeq 0.2$ at the Reynolds number $Re_D = 1700$.

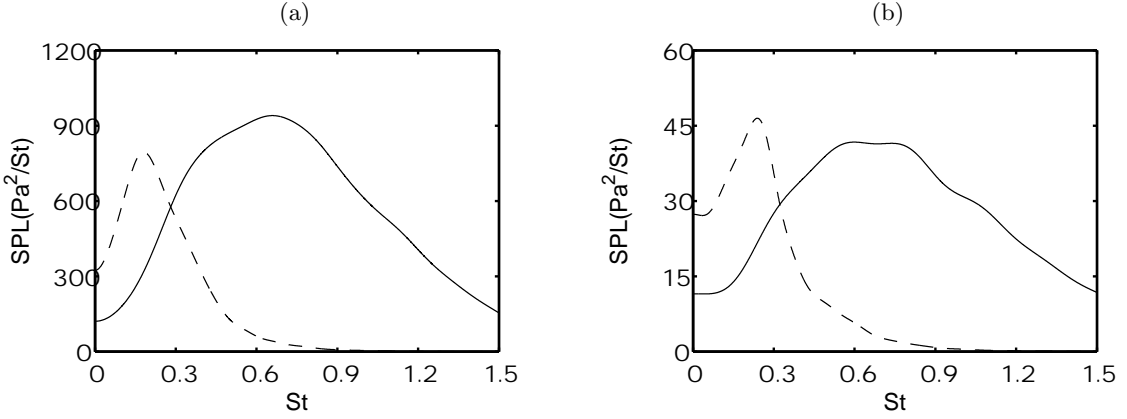


Figure 4. Pressure spectra obtained at the point M_{90} as a function of Strouhal number $St = fD/u_j$: (a) Mach 0.9 jets, (b) Mach 0.6 jets; at: — high Reynolds number, - - - $Re_D = 1700$.

III. Results

A. Correlations between pressure at M_{40} and jet turbulence

1. Case $M_{40}/axis$

The normalized cross-correlations between the fluctuating pressure at point M_{40} at 40° to the jet axis and the turbulence signals u' , v' , u'^2 , v'^2 , w'^2 , k and $|\boldsymbol{\omega}|$ along the jet axis are represented in figure 5 for the different jets. The correlations with the fluctuating velocity w' are not presented because they are found to be negligible. At a given Reynolds number, the correlation maps provided by the jets at Mach 0.9 and 0.6 are very similar. This is visible both at $Re_D \geq 10^5$ in figures 5(a) and 5(c), and at $Re_D = 1700$ in figures 5(b) and 5(d). Among the correlations presented, the correlations Cvp in figures 5(2), obtained from the radial velocity v' , appear to have the lower levels. All the other ones display large zones with levels noticeably higher than 0.04. The correlations with the axial fluctuating velocity u' , Cup , in figures 5(1), show significant values of both positive and negative signs, whereas the correlations with the Reynolds stresses, the turbulent kinetic energy and the vorticity norm are dominated by positive values, especially at the low Reynolds number of $Re_D = 1700$. In addition, the higher correlation levels are observed in the vicinity of the end of the potential core, indicated by an horizontal dotted line. They also occur for time delays close to the time corresponding to a propagation between the centerline points and the point M_{40} at the speed of sound in the ambient medium, which is given by a vertical solid line. The latter points are for instance remarkably illustrated by the correlations with the vorticity norm, $C|\boldsymbol{\omega}|p$, for the LESm09re1700 jet in figure 5(7)(b). In this case, the maximum correlation is found at the point of intersection of the solid and dotted lines.

The space/time position of the maximum correlations is investigated more quantitatively in figures 6 and 7. In figures 6, the axial profiles of the peaks of $-Cup$, $Cuup$ and $C|\boldsymbol{\omega}|p$, are represented for the different jets. In all cases, the maximum is observed near the end of the potential core. The axial location of the maximum correlations is in particular very close to $x = x_c$ for the jets at $Re_D = 1700$ in figures 6(b) and 6(d). At the high Reynolds numbers $Re_D \geq 10^5$, the maximum correlations appear however slightly upstream, e.g. in figures 6(1)(a) and 6(1)(c) for the peaks of $-Cup$.

The cross-correlation functions between pressure at point M_{40} and velocity u' at $x = x_c - 2r_0$, Reynolds stresses u'^2 and vorticity norm $|\boldsymbol{\omega}|$ at $x = x_c$ on the jet centerline are given in figures 7. The shapes of the

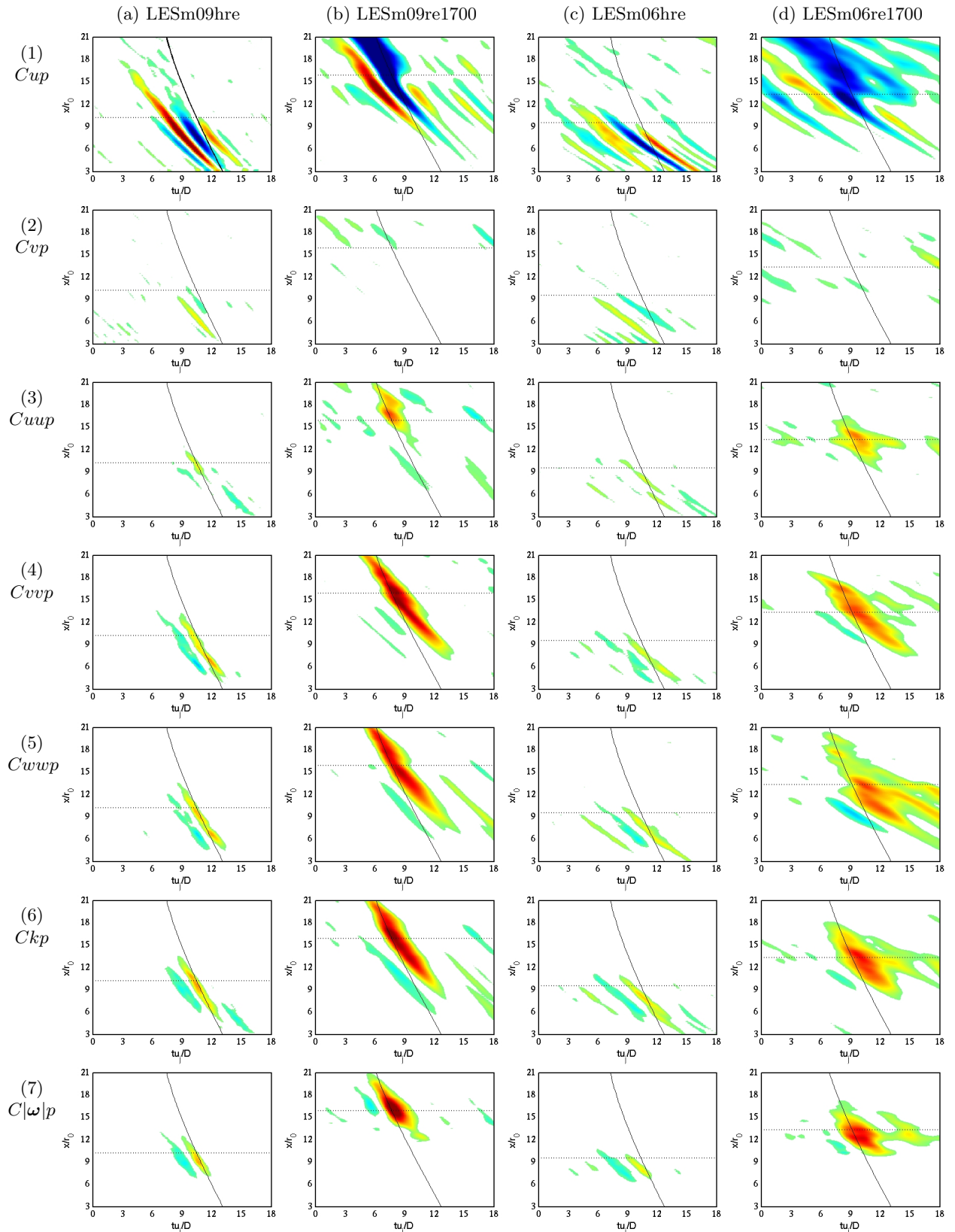


Figure 5. Case $M_{40}/axis$. Normalized cross-correlations between pressure at M_{40} and flow quantities along jet axis: (1) C_{up} , (2) C_{vp} , (3) C_{uup} , (4) C_{vvp} , (5) C_{wvp} , (6) C_{kp} , (7) $C|\omega|p$, obtained for the jets: (a) LESm09hre, (b) LESm09re1700, (c) LESm06hre, (d) LESm06re1700 (X-axis: non-dimensional time delay tu_j/D , Y-axis: axial distance x/r_0). The color scale is defined from -0.14 to 0.14 , with white in the range $[-0.035, 0.035]$. The solid line represents the propagation time between the centerline points and the point M_{40} at the sound speed. The dotted line shows the end of the potential core.

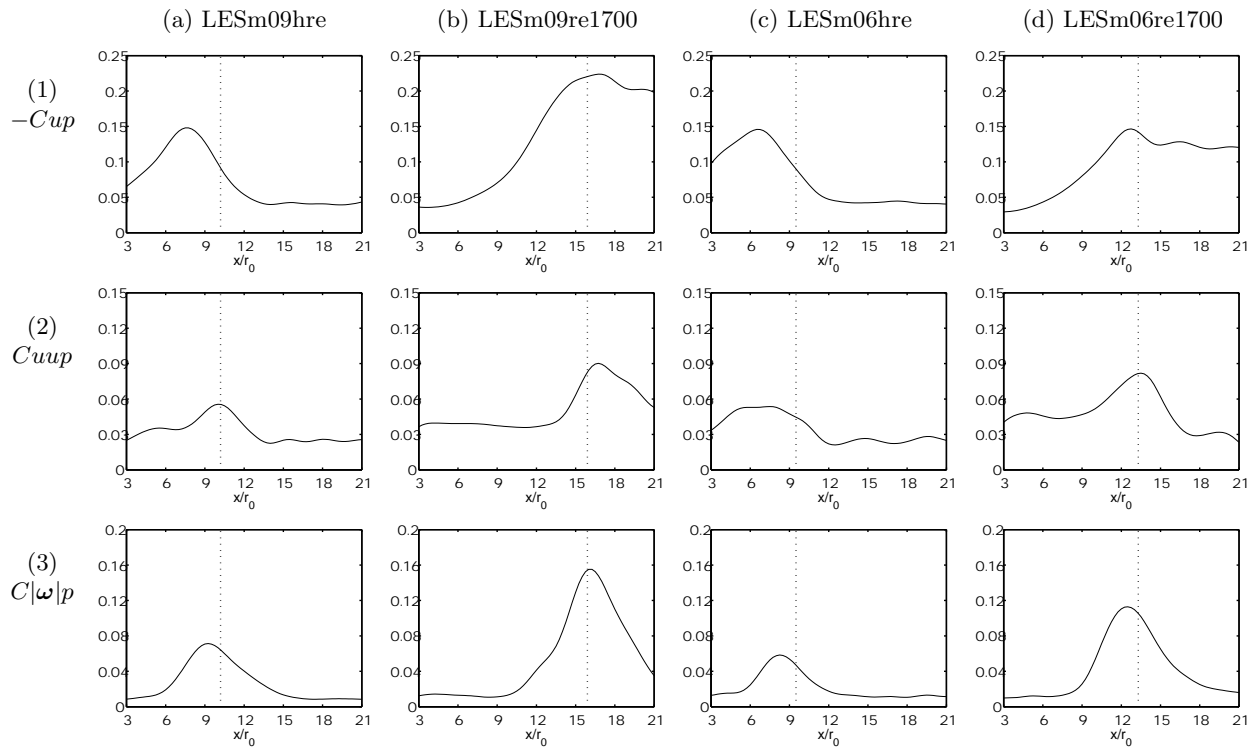


Figure 6. Case $M_{40}/axis$. Axial variation of peak correlation between pressure at M_{40} and flow quantities along jet axis. Peaks of: (1) $-C_{up}$, (2) C_{wup} , (3) $C|\omega|p$, for the jets: (a) LESm09hre, (b) LESm09re1700, (c) LESm06hre, (d) LESm06re1700. The dotted line shows the location of the end of the potential core.

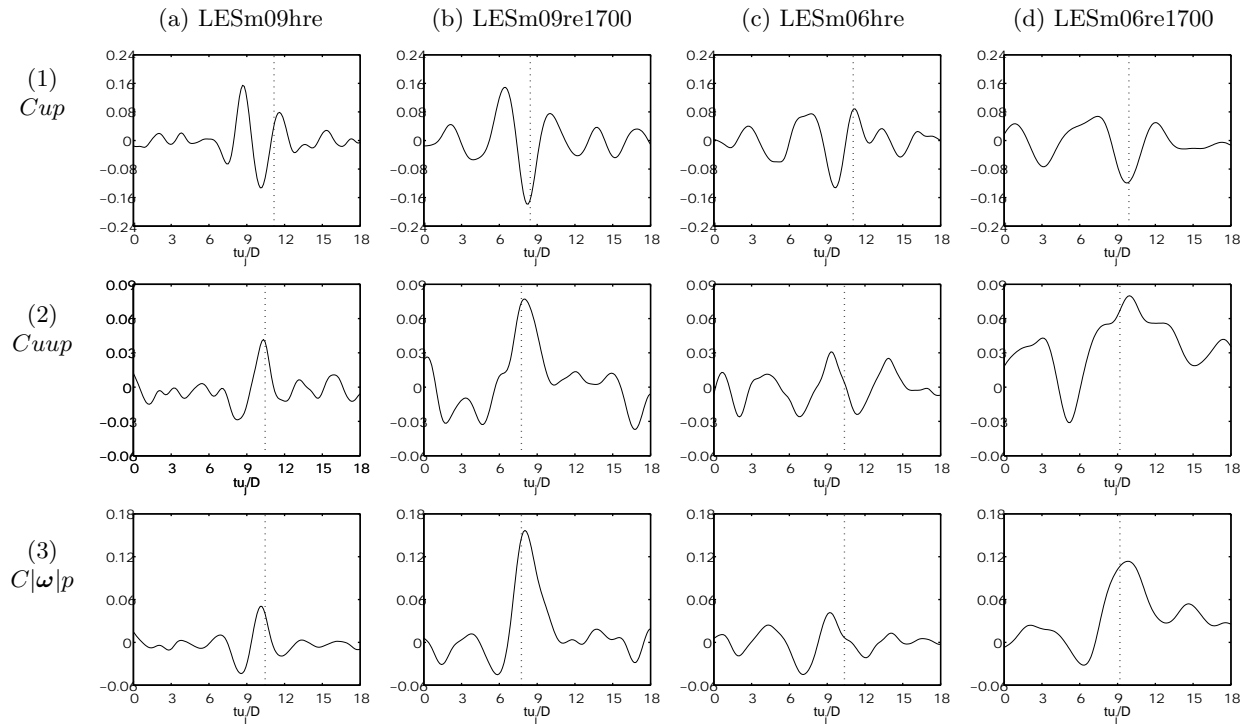


Figure 7. Case $M_{40}/axis$. Normalized cross-correlations between pressure at M_{40} and flow quantities on the jet axis: (1) C_{up} for a centerline point at $x = x_c - 2r_0$, (2) C_{wup} for a point at $x = x_c$, (3) $C|\omega|p$ for a point at $x = x_c$, for the jets: (a) LESm09hre, (b) LESm09re1700, (c) LESm06hre, (d) LESm06re1700 (X-axis: non-dimensional time delay tu_j/D). The dotted line represents the time delay for a propagation at the sound speed between the centerline point and the point M_{40} .

correlation functions $Cuup$ and $C|\omega|p$ are similar, and exhibit a peak at a time delay corresponding nearly to the time of propagation at the speed of sound between the two observation points considered. Those of the correlations Cup are basically different with a positive peak followed by a negative peak located fairly well at the propagation time delay, as shown for instance in figure 7(1)(b) for the LESm09re1700 jet. The present correlation curves are in good agreement with the experimental data obtained by Schaffar²² for a jet at $M = 0.98$ between pressure at 30° to the jet axis and centerline turbulence at the end of the jet core.

As for the levels of the maximum correlations between pressure at point M_{40} and centerline turbulence, they are provided in table 2 with the maxima of $-Cup$, $Cuup$, $Cvvp$, $Cwvp$, Ckp and $C|\omega|p$ for the different simulated jets. Their variations with the Mach and Reynolds numbers are thus shown. In all the cases reported, the correlations decrease as the Mach number is reduced from $M = 0.9$ down to $M = 0.6$. This trend is in agreement with the experimental data of Hurd *et al.*¹⁶ and Panda *et al.*^{23,24} Furthermore the correlations are higher at the low Reynolds number $Re_D = 1700$ than at the high Reynolds numbers $Re_D \geq 10^5$. These effects of the Mach and Reynolds numbers are clearly illustrated in figure 8 by the axial variations of the peak of $C|\omega|p$ for the different jets.

In table 2, the higher values are obtained for the maxima of $-Cup$, which are around 0.15. The maximum correlations calculated from the signals of Reynolds stresses u'^2 , v'^2 , w'^2 , turbulent kinetic energy k and vorticity norm $|\omega|$ are moreover rather close, with for instance levels between 0.06 and 0.08 for the LESm09hre jet. These turbulence signals can therefore be expected to display a common characteristic accounting for these similar results. It is difficult to check the present levels from the experimental data of the literature, which were often filtered cross-correlations for jets at low Mach numbers.¹⁷⁻²¹ The only relevant data are the broadband correlations provided by Schaffar²² for a jet at $M = 0.98$, between pressure at 30° to the jet axis and signals of u' and u'^2 on the jet axis. Schaffar²² thus obtained peaks of $-Cup$ and $Cuup$ of about 0.06 and 0.04, respectively. These values are significantly lower than our findings for the LESm09hre jet. This discrepancy may be due to the high Reynolds number of the jet studied by Schaffar.²² At $Re_D = 9 \times 10^5$, his jet is certainly fully turbulent at the nozzle exit,³¹ and parasitic velocity fluctuations are likely to be found in the jet core on the centerline. This may decrease the correlation levels with respect to the case where the jet is initially transitional, as in our simulations.

Table 2. Case $M_{40}/axis$. Maximum correlations between pressure at point M_{40} and flow quantities along jet axis. The subscript m is used for *maximum*.

	$(-Cup)_m$	$(Cuup)_m$	$(Cvvp)_m$	$(Cwvp)_m$	$(Ckp)_m$	$(C \omega p)_m$
LESm09hre	0.155	0.059	0.084	0.076	0.082	0.077
LESm09re1700	0.230	0.098	0.144	0.131	0.145	0.168
LESm06hre	0.153	0.057	0.059	0.064	0.071	0.063
LESm06re1700	0.155	0.087	0.103	0.102	0.115	0.118

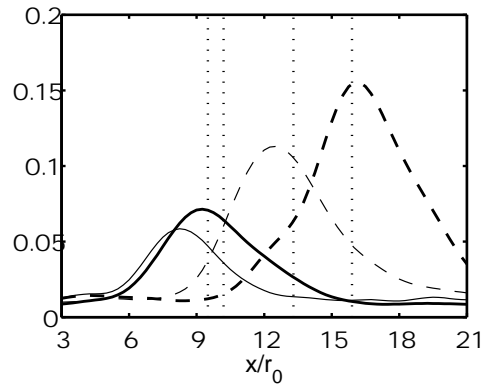


Figure 8. Case $M_{40}/axis$. Axial variation of peak correlation between pressure at M_{40} and vorticity norm along jet axis (peak of $C|\omega|p$), for the jets: — LESm09hre, - - - LESm09re1700, — — — LESm06hre, - · - · LESm06re1700. The dotted line shows the location of the end of the potential core for the different jets.

2. Case $M_{40}/\text{shear-layer}$

The normalized correlations between pressure at downstream observation point M_{40} and the signals of fluctuating velocity u' and Reynolds stresses u'^2 , v'^2 and w'^2 along the shear layer are represented in figure 9. The correlations involving other turbulence quantities are not shown here because they are much smaller. The correlations presented are themselves weak. At high Reynolds numbers in figures 9(a) and figures 9(c), they even seem negligible, which agrees well with the measurements of Panda *et al.*^{23,24} displaying very weak correlation between shear-layer turbulence and pressure at 30° to the jet axis for a high-Reynolds-number jet at $M = 0.95$. At $Re_D = 1700$ in figures 9(a) and figures 9(c), the correlation levels are however higher, especially for $Cvvp$ and $Cwvp$ calculated from the Reynolds stresses v'^2 and w'^2 . In these two cases, the peak correlations appear in the vicinity of the end of the potential core, at a time delay in good agreement with the propagation time delay, as in the previous case $M_{40}/\text{jet axis}$, but exhibit lower values.

These observations are supported in figures 10 by the axial variations of the peaks of $Cvvp$ and $Cwvp$. At high Reynolds numbers, no significant peak can be distinguished from the floor noise of about 0.03. At the low Reynolds number of $Re_D = 1700$, the correlation levels are higher in the region near the end of the jet core. The maximum correlations are about 0.06 for the jet at Mach 0.9 and 0.05 for the jet at Mach 0.6. These values are noticeably lower than the maximum correlations obtained between pressure at point M_{40} and centerline Reynolds stresses, which are about 0.14 for the LESm09re1700 jet at $M = 0.9$ and 0.10 for the LESm06re1700 jet at $M = 0.6$, as reported in table 2.

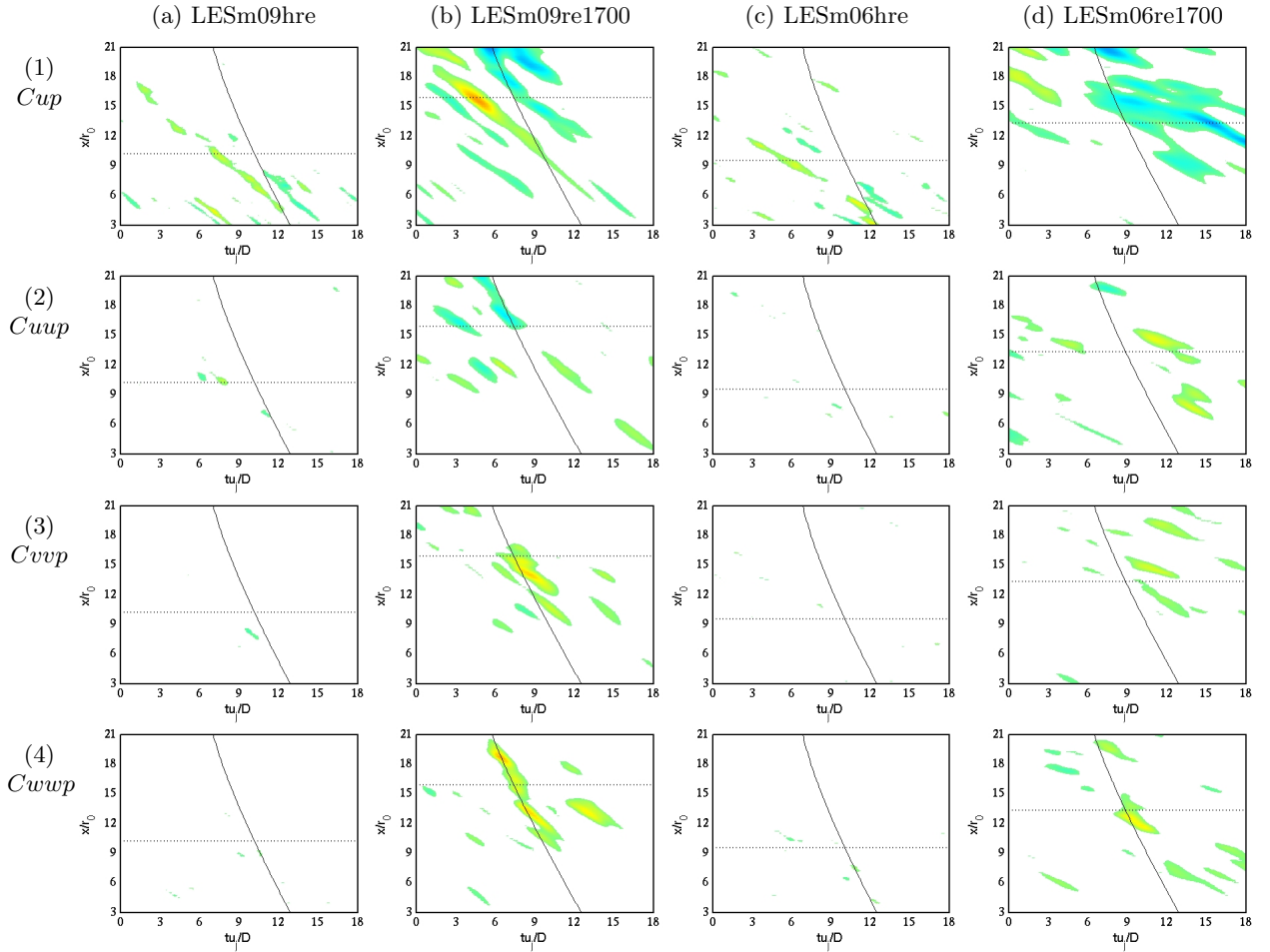


Figure 9. Case $M_{40}/\text{shear-layer}$. Normalized correlations between pressure at M_{40} and flow quantities along shear layer: (1) C_{up} , (2) C_{uup} , (3) C_{vvp} , (4) C_{wvp} , for the jets: (a) LESm09hre, (b) LESm09re1700, (c) LESm06hre, (d) LESm06re1700 (X-axis: non-dimensional time delay tu_j/D , Y-axis: axial distance x/r_0). The color scale is defined from -0.14 to 0.14, with white in the range [-0.035 0.035]. The solid line represents the propagation time between the shear-layer points and the point M_{40} at the sound speed. The dotted line shows the end of the jet core.

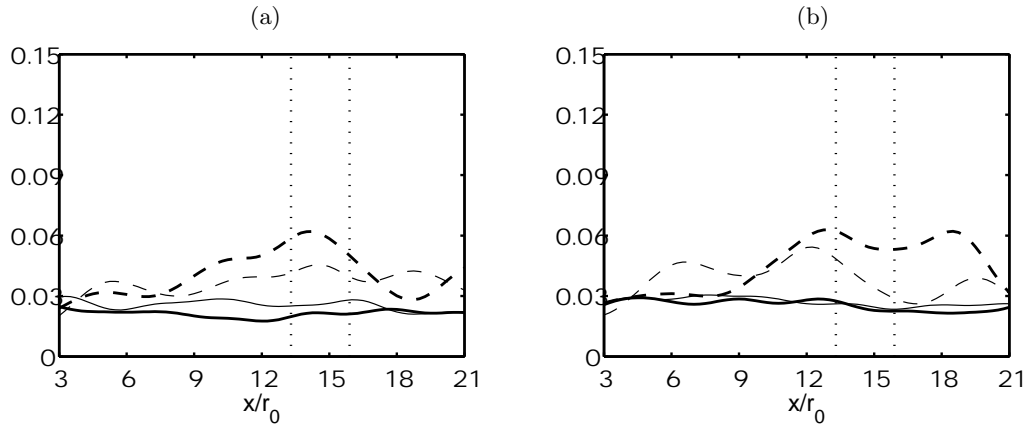


Figure 10. Case M_{40} /shear-layer. Axial variation of peak correlation between pressure at M_{40} and flow quantities along shear layer. Peaks of: (a) $Cvvp$, (b) $Cwvp$, for the jets: — LESm09hre, - - - LESm09re1700, — — LESm06hre, - - - LESm06re1700. The dotted line shows the location of the end of the potential core for the jets at $Re_D = 1700$.

B. Correlations between pressure at M_{90} and jet turbulence

1. Case M_{90} /shear-layer

The normalized cross-correlations between pressure at point M_{90} at 90° to the jet axis, relative to the end of the potential core, and signals of fluctuating velocity u' , and Reynolds stresses u'^2 and v'^2 , along shear layer, are presented in figure 11. The correlation levels are found to be very weak for the jets at high Reynolds numbers in figures 11(a) and 11(c), as well as for the jets at $Re_D = 1700$ in figures 11(b) and 11(d). Note also that negligible correlations with pressure at point M_{90} are observed using any turbulence quantity in the shear layer.

Exhibiting causality links between sideline pressure and shear-layer turbulence therefore appears difficult using broadband direct cross-correlations, although measurements suggested that a significant part of sideline noise is generated in the jet shear-layer.¹¹ These weak correlation levels certainly arise from the fact that the noise components predominant in the sideline direction are due the randomly-developing turbulence,^{6,10} over an extended source region as pointed out by Seiner.¹⁸

2. Case M_{90} /axis

Finally, the normalized correlations between the fluctuating pressure at the sideline point M_{90} and the turbulence signals u' , u'^2 and $|\omega|$ along jet axis are presented in figure 12. For brevity the correlations calculated from the Reynolds stresses v'^2 and w'^2 , and from the turbulent kinetic energy k are not provided. However they show correlation maps similar to those obtained from the vorticity norm in figures 12(3). The correlation levels are negligible for the high-Reynolds-number jets in figures 12(a) and 12(c), but they are found to be significant for the jets at $Re_D = 1700$ in figures 12(b) and 12(d). In the latter case, large zones exhibiting correlation levels higher than 0.04 are observed. As previously with the correlations involving the downstream observation point M_{40} , the maximum levels are observed in the vicinity of the end of the potential core. They also occur for time delays fairly close to the time of propagation at the speed of sound between the aerodynamic and acoustic observation points considered. Moreover, with respect to the case M_{40} /axis in section III.A.1., where centerline turbulence is correlated with pressure at the downstream point at 40° to the jet axis, the peaks appear of opposite signs. Compare for instance the $Cuup$ correlations obtained for the LESm09re1700 jet, reported in figure 12(2)(b) for the present case and in figure 5(2)(b) for the case M_{40} /axis: negative and positive peaks are respectively observed.

The correlations between the fluctuating pressure at point M_{90} and the signals of u' at $x = x_c + r_0$, and of u'^2 and $|\omega|$ at $x = x_c - r_0$ on the jet axis are now presented in figures 13. As expected from figures 12, the correlations are very weak in figures 13(a) and 13(c) for the jets at high Reynolds numbers. For the jets at $Re_D = 1700$, in figures 13(c) and 13(d), the correlations Cup show a positive peak at about the propagation time delay, preceded by a positive peak with a similar level. The correlations $Cuup$ and $C|\omega|p$ display the

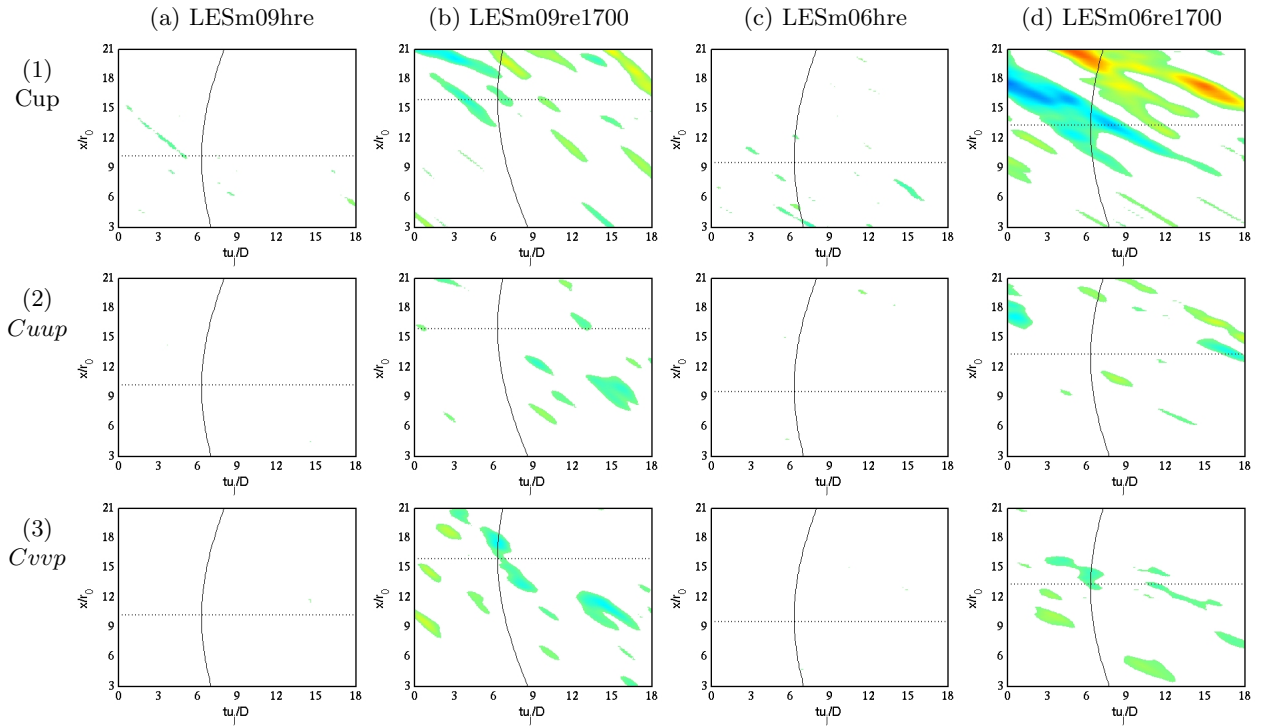


Figure 11. Case M_{90} /shear-layer. Normalized correlations between pressure at M_{90} and flow quantities along shear layer: (1) C_{up} , (2) C_{uup} , (3) C_{vvp} , for the jets: (a) LESm09hre, (b) LESm09re1700, (c) LESm06hre, (d) LESm06re1700 (X-axis: non-dimensional time tu_j/D , Y-axis: axial distance x/r_0). The color scale is defined from -0.14 to 0.14, with white in the range $[-0.035, 0.035]$. The solid line represents the propagation time delay between the shear-layer points and the point M_{90} at the sound speed. The dotted line shows the end of the jet core.

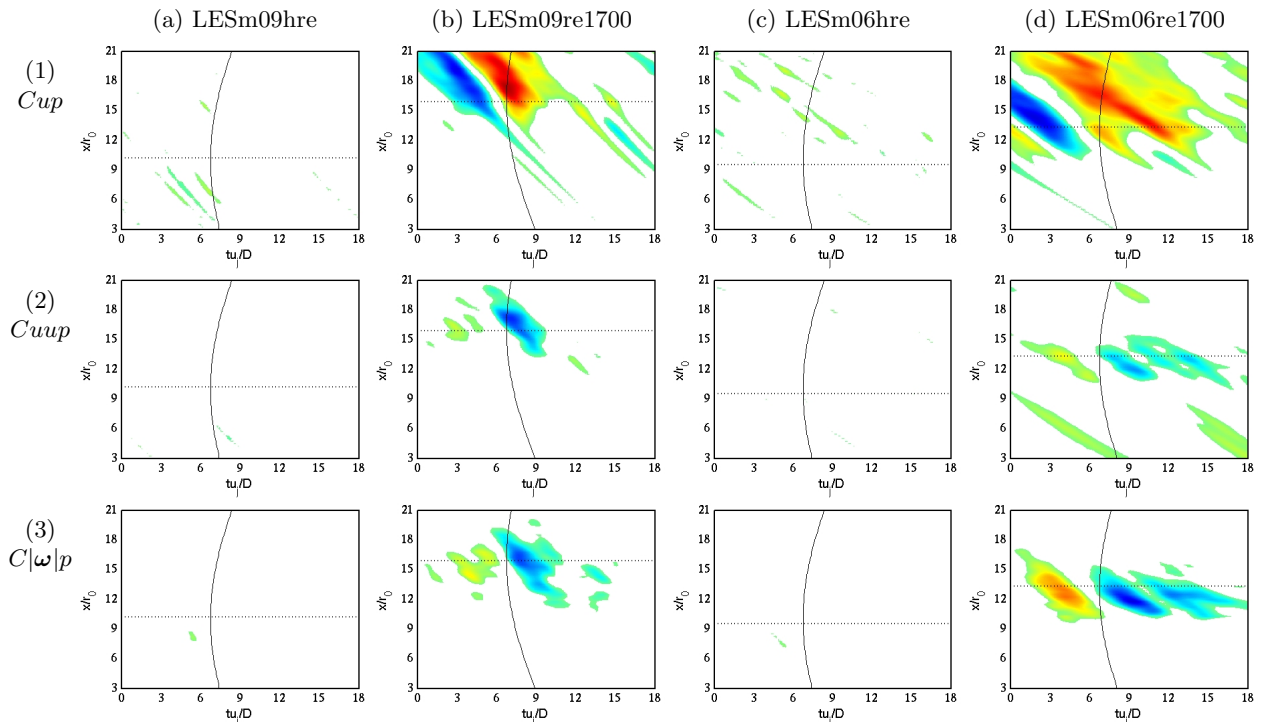


Figure 12. Case M_{90} /axis. Normalized correlations between pressure at M_{90} and flow quantities along jet axis: (1) C_{up} , (2) C_{uup} , (3) $C_{|\omega|p}$, for the jets: (a) LESm09hre, (b) LESm09re1700, (c) LESm06hre, (d) LESm06re1700. See also the caption of figure 11 above.

opposite case: the peak nearly at the propagation time is negative, and the preceding is positive. As for the peak levels, they are about 0.08-0.10. They are lower than the peak levels obtained in the case M_{40}/axis , which are in the range 0.10-0.15. In addition, no appreciable effect of the Mach number can be convincingly found between the present results at Mach 0.9 and Mach 0.6.

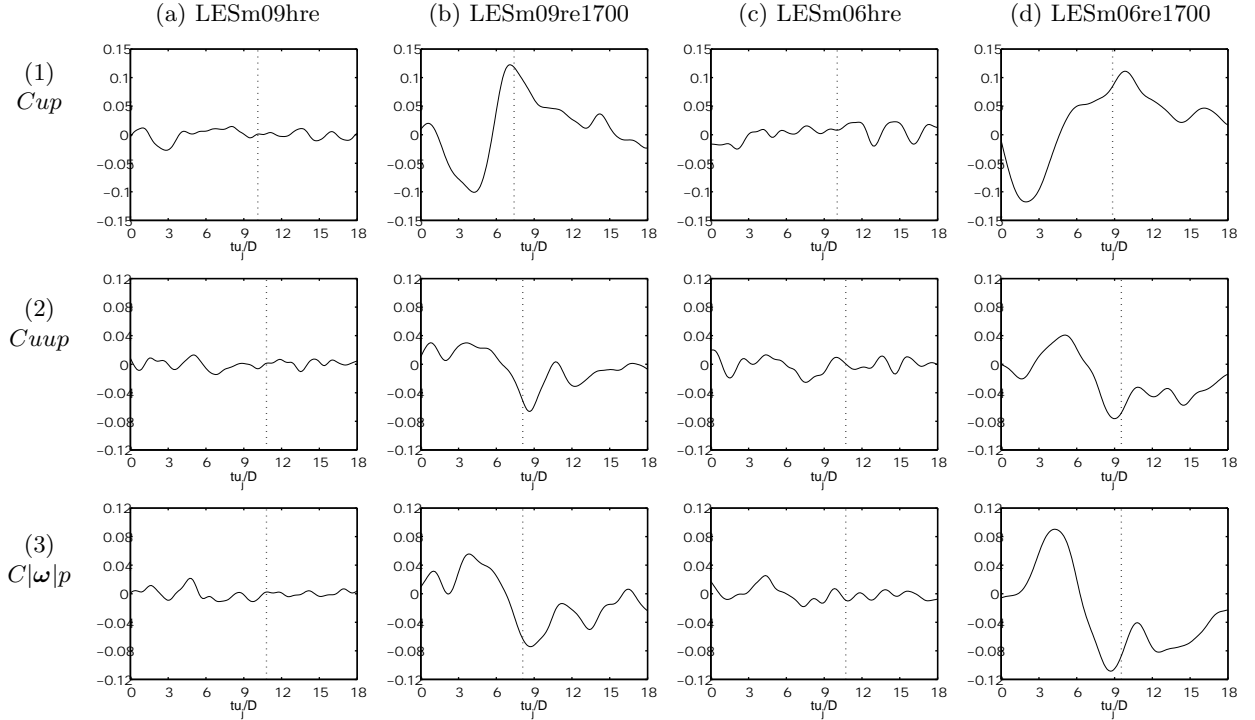


Figure 13. Normalized cross-correlations between pressure at M_{90} and flow quantities on the jet axis: (1) C_{up} for a centerline point at $x = x_c + r_0$, (2) C_{wup} and (3) $C_{|\omega|p}$ for a point at $x = x_c - r_0$, for the jets: (a) LESm09hre, (b) LESm09re1700, (c) LESm06hre, (d) LESm06re1700 (X-axis: non-dimensional time delay tu_j/D). The dotted line represents the time delay for a propagation at the sound speed between the centerline point and the point M_{90} .

C. Properties of centerline turbulence

In this section, the properties of the centerline turbulence, for which the maximum correlations are obtained with the radiated pressure, are briefly investigated.

1. Spectral properties

The spectral content of the centerline turbulence is first studied. The spectra of the fluctuating radial velocity v' obtained on the jet axis at the end of the potential core, at $x = x_c$, are presented in figures 14(a) and 14(b) for the jets at Mach 0.9 and Mach 0.6, respectively. At both Mach numbers, the spectra are dominated by frequency peaks at the low Strouhal numbers of $St \simeq 0.3$ at the high Reynolds numbers $Re_D \geq 10^5$, and of $St \simeq 0.2$ at $Re_D = 1700$. The peaks are however more marked for the high-Reynolds-number jets. The peak frequencies of the present spectra of velocity at the end of the jet core are in good agreement with the peak Strouhal numbers of the downstream sound pressure spectra obtained at about 30° to the jet axis, which are given in a previous paper.¹⁰ They further agree with the peaks observed in the pressure spectra at 40° to the jet axis for the $M = 0.9$ jets, as shown in figure 3(a).

The variations of the peak Strouhal in the spectra of centerline v' velocity are now presented in figures 15(a). The magnitudes associated with the peaks are also provided in figure 15(b), showing the rapid increase of the turbulence intensity at the end of the potential core. For the different simulated jets, the peak Strouhal number is found not to vary much in the region extending from two diameters upstream of the end of the potential core to two diameters downstream. This observation suggests the occurrence, at the end of the potential core on the jet axis, of a turbulence phenomenon that is persistent over a large distance.

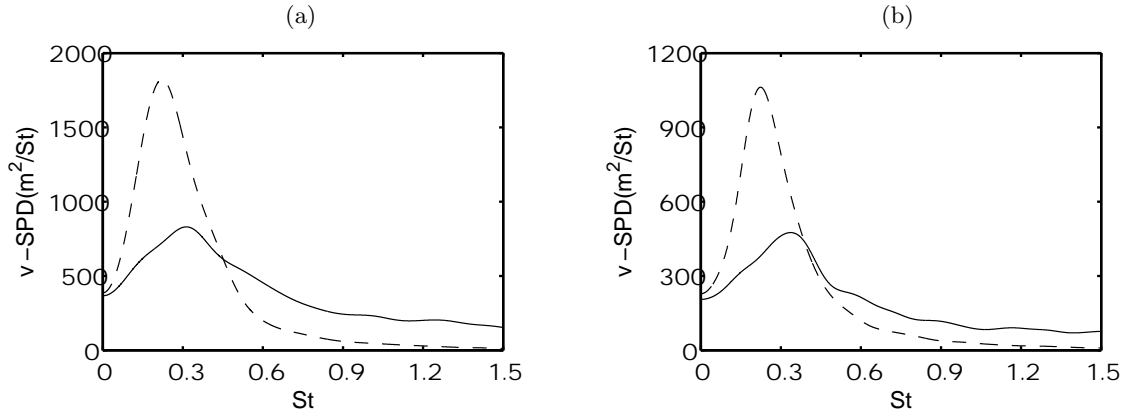


Figure 14. Spectral power densities of v' velocity as a function of Strouhal number $St = fD/u_j$, at $x = x_c$ on the jet axis: (a) Mach 0.9 jets, (b) Mach 0.6 jets; at: — high Reynolds number, - - $Re_D = 1700$.

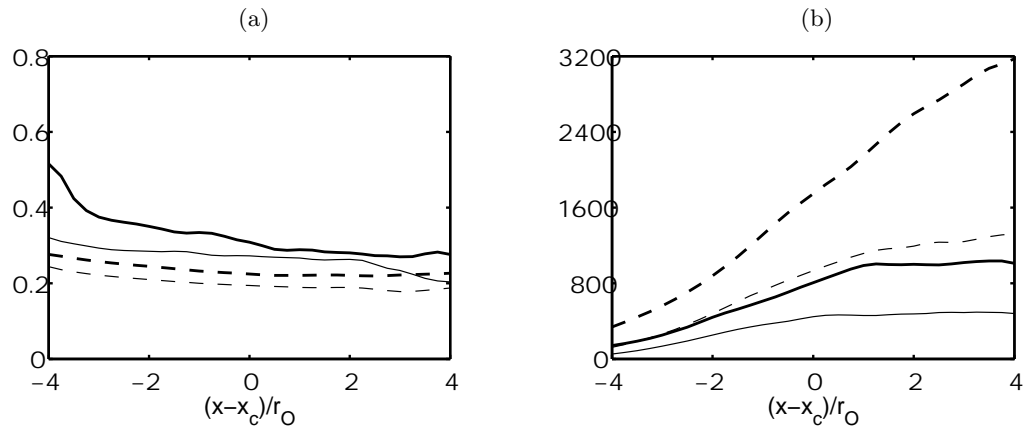


Figure 15. (a) Strouhal number, and (b) level (in m^2 per St), of the peak in v' -velocity spectra on the jet axis, as a function of $x - x_c$, the axial position with respect to the end of the potential core, for the jets: — LESm09hre, - - - LESm09re1700, — LESm06hre, - - - LESm06re1700.

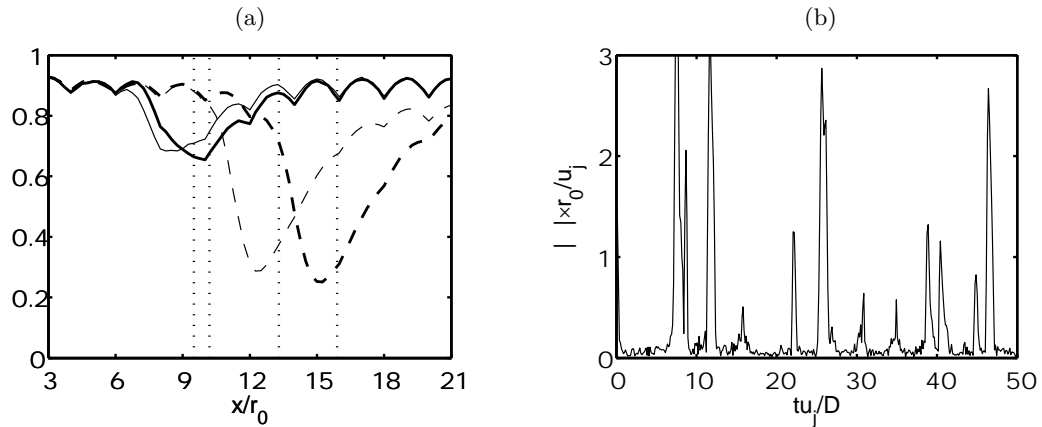


Figure 16. Intermittency on the jet axis. (a) Intermittency factor γ along the jet axis, calculated from the vorticity norm $|\omega|$, for the jets: — LESm09hre, - - - LESm09re1700, — LESm06hre, - - - LESm06re1700. (b) Time evolution of the vorticity norm $|\omega| \times r_0/u_j$ at $x = x_c$ on the jet axis, for the LESm09re1700 jet.

2. Intermittency

The features of the flow phenomena at the end of the potential core are now investigated through intermittency.³² In the literature, the intermittency of momentum and heat transport in turbulent round jets was for instance studied by Chevray & Tutu.³³ The intermittency of the noise emission in subsonic jets was also shown by Juvé *et al.*²⁰ thanks to the use of a conditional sampling procedure in the calculation of cross-correlations between far-field acoustic pressure at 30° to the jet direction and velocity fluctuations in a $M = 0.4$ jet.

In the present work, the intermittency of the centerline turbulence is analyzed by means of the function $I(t)$ defined arbitrarily from the vorticity norm $|\omega|$ by

$$I(t) = \begin{cases} 1 & \text{if } |\omega| \text{ higher than } \langle |\omega| \rangle / 2 \\ 0 & \text{otherwise} \end{cases}$$

which allows to determine the intermittency factor $\gamma = \langle I(t) \rangle$. This γ factor is based on the vorticity norm, but Reynolds stresses or turbulent kinetic energy can be used in the same way. It is expected to be $\gamma \simeq 1$ when the vorticity signal is turbulent, but $\gamma \simeq 0$ when the signal is intermittent.

The intermittency factor γ , calculated along the jet centerline from the vorticity norm $|\omega|$ as described above, is represented in figure 16(a). For the four simulated jets, the factor γ is about 1 in the first part of the potential core, and displays a noticeable decrease near the end of the core, down to about 0.25 for the LESm09re1700 jet, with a minimum located slightly upstream of $x = x_c$. Farther downstream, the factor γ increases progressively to recover finally values close to 1. The vorticity signal is therefore significantly intermittent in the vicinity of the end of the jet core. The intermittency level is found to be a little higher at Mach 0.9 than at Mach 0.6. It also increases appreciably as the Reynolds number is reduced down to $Re_D = 1700$. Moreover, there is a good similarity between the variations of the intermittency of centerline vorticity norm $|\omega|$, in figure 16(a), and those of the peak of the correlations $C|\omega|p$ between pressure at point M_{40} and centerline vorticity, in figure 8. The higher the intermittency, the higher the maximum correlation.

The intermittency of centerline turbulence is illustrated in figure 16(b) by the time evolution of the vorticity norm $|\omega|$ at $x = x_c$ on the jet axis, for the LESm09re1700 jet. Turbulence appears to be intermittently, and periodically, present on the jet axis at the end of the potential core. The associated non-dimensional period is between 4 and 5, which is in good agreement with the peak Strouhal number obtained in the spectra of velocity v' , in figures 14(a) and 15(a). This phenomenon of intrusion of vortical structures into the jet core was described by the authors from results of a previous jet simulation.¹⁴ It was also connected to the sound waves radiated in the downstream direction. The present results strongly support this view. The deterministic source responsible for the downstream jet noise component¹⁰ is therefore likely to be this mechanism intrinsic to the jet geometry at the end of the potential core.

To show how the intermittent signals of turbulence can provide significant correlations with the pressure radiated downstream, the time evolutions of vorticity $|\omega|$ at $x = x_c$ on the jet axis, and of pressure p' at point M_{40} , are both represented in figure 17(a) for the LESm09re1700 jet. The pressure signal is given at the retarded time taking account of the propagation time delay at the speed of sound between the two observation points. The bursts of vorticity appear to be well correlated with positive pressure fronts, which yields the positive correlation peak obtained in figures 5(7)(b) and 7(3)(b). Identical observations could be made with the signals of Reynolds stresses and turbulence kinetic energy, which all are positive quantities, and exhibit similar cross-correlations with the radiated pressure.

For the fluctuating axial velocity u' , the case is different: the intrusion of vortical structures in the jet core results in a velocity deficit. Strong negative peaks of u' , more marked than those attributed to random turbulent motions, then occur intermittently. These peaks are clearly observed in figure 17(b) where the signal of velocity u' is presented for the LESm09re1700 jet at the same time as vorticity norm in figure 17(a) above. They correlate with the positive fronts of the pressure signal at point M_{40} , which is represented at the appropriate retarded time as previously. This gives the significant negative correlations obtained in figures 5(1)(b) and 7(1)(b). Note that these results agree with the experimental observations of Juvé *et al.*²⁰ who noticed that, for points located near the end of the potential core, the periods of noise generation appear to coincide frequently with a marked deceleration of the flow. Finally, for the fluctuating velocities v' and w' , the intermittency at the end of the jet core does not produce remarkable deviations in the signals. Fluctuations v' and w' are therefore only associated with the random motions of vortical structures, which leads to the weak cross-correlations with the radiated pressure.

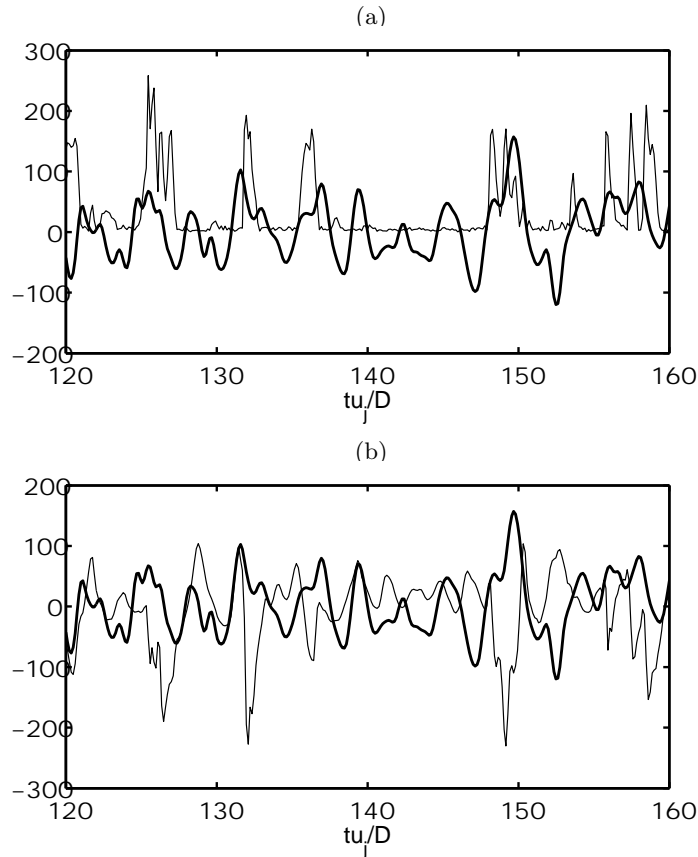


Figure 17. Time evolution, for the LESm09re1700 jet: —, (a) vorticity norm $|\omega| \times r_0/u_j \times 70$ and (b) fluctuating velocity $u'/u_j \times 600$, at $x = x_c$ on the jet axis; — fluctuating pressure p' (in Pa) at the point M_{40} , at the retarded time corresponding to a propagation at the sound speed between the centerline point and the point M_{40} .

As for the correlations observed at the low Reynolds number of $Re_D = 1700$ between centerline turbulence and sideline pressure at point M_{90} , their different shapes with respect to the case at downstream point M_{40} may be linked to the features of the pressure signals at 90° to the jet axis. These correlations may further indicate that the intermittent jet noise source does not contribute in a negligible manner to the radiated sideline noise at the low Reynolds number $Re_D = 1700$.

D. Correlations between pressure and turbulence at the end of the jet core

The variations with the emission angle of the correlations between radiated pressure and centerline turbulence at the end of the potential core are finally investigated for the high-Reynolds-number jets. Normalized correlations are thus calculated between turbulence signals at $x = x_c$ on the jet axis, and pressure at the different acoustic observation points presented in figure 1. The peaks of cross-correlations Cup and $C|\omega|p$, involving velocity u' and vorticity norm $|\omega|$, are plotted respectively in figures 18(a) and 18(b), as functions of the emission angle θ relative to the end of the jet core, for the high-Reynolds-number jets at $M = 0.9$ and $M = 0.6$. In both cases, the correlations are significantly higher with the pressure radiated in the downstream direction. The correlation levels are observed to decrease dramatically with the emission angle. They are even negligible for $\theta \geq 75^\circ$. This behaviour is in agreement with the experimental data provided for high-Reynolds-number jets by Hurd *et al.*¹⁶ and Panda *et al.*²⁴

The angular dependence of the correlations between pressure and turbulence at the end of the jet core brings us some information about the contribution of the intermittent sound source to the radiated noise for the high-Reynolds-numbers jets considered. This contribution is found to be very important at small radiation angles, but negligible in the sideline direction, which is in agreement with the source directivity suggested by other works.^{6,10}

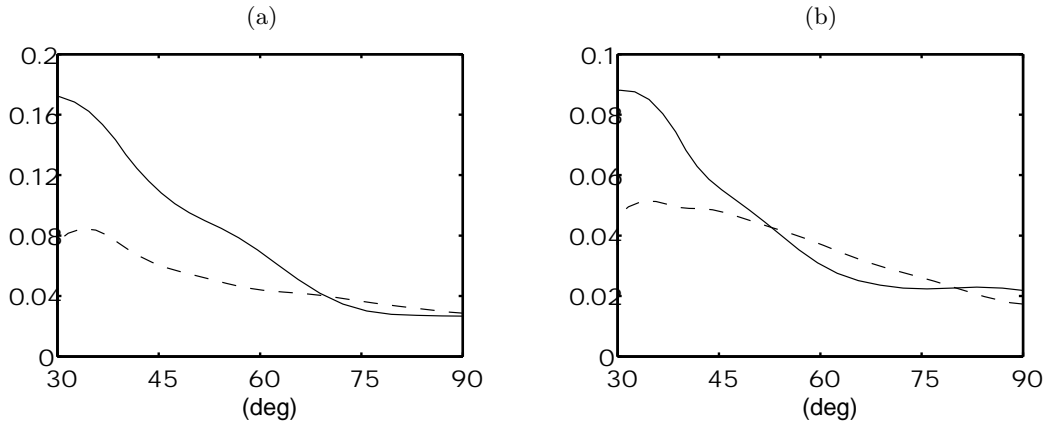


Figure 18. Angular variation of peak correlation between radiated pressure and flow quantities at $x = x_c$ on the jet axis (θ : angle with respect to the jet direction). Peaks of: (a) C_{up} , (b) $C_{|\omega|p}$, for the high-Reynolds-number jets: — LESm09hre, - - - LESm06hre.

IV. Summary and conclusion

In the present paper, noise sources are investigated using the causality method in subsonic round jets computed by Large Eddy Simulation, at Mach numbers $M = 0.6$ and $M = 0.9$, at the low and high Reynolds numbers of $Re_D = 1700$ and $Re_D \geq 10^5$. Normalized cross-correlations between the broadband signals of jet turbulence and of radiated pressure, provided directly by the simulations, are presented. The turbulence quantities considered here are the fluctuating velocities, the Reynolds stresses, the turbulent kinetic energy and the vorticity norm. Correlations are in particular calculated using the pressure obtained at the radiation angles, relative to an origin at the end of the potential core, of 40° and 90° from the jet direction, and turbulence along the jet axis and along the shear layer.

For the pressure radiated at 40° to the jet axis, significant correlations are obtained with the centerline turbulence for all the simulated jets. Peak correlations are observed at the end of the potential core, for time delays corresponding fairly well to the time of propagation at the speed of sound between the source and the emission points. The maximum correlations are between 0.06 and 0.15 for the jets at high Reynolds numbers $Re_D \geq 10^5$. They are higher for the jets at the low Reynolds number of $Re_D = 1700$. They also decrease as the Mach number is reduced. The correlations between pressure at 40° to the jet axis and turbulence along the shear layer are considerably smaller. They reach a maximum of only 0.06 for the jets at $Re_D = 1700$, and are even negligible for the high-Reynolds-number jet.

For the sideline pressure at 90° to the jet axis, the correlations with the shear-layer turbulence are found to be insignificant for all the computed jets. The cross-correlations with the centerline turbulence are also weak, especially for the high-Reynolds-number jets. They are however appreciable for the jets at $Re_D = 1700$. In that case, maximum correlation levels of about 0.10 are obtained at the end of the jet core.

The present results support the presence of a noise generation mechanism near the end of the potential core, on the jet centerline. The correlations moreover suggest that the contribution of this sound source to the radiated noise is important in the downstream direction, but very small in the sideline direction, except maybe at very low Reynolds numbers. Considering this feature, the noise source in question is likely to be the source responsible for the downstream jet noise component exhibited in experimental and numerical works. The signals of turbulence at the end of the jet core moreover show that this source is characterized by a dominant low-Strouhal-number frequency over a large axial distance and by a high level of intermittency. The periodic and intermittent intrusion of vortical structures into the jet core, and consequently their sudden acceleration, can therefore be expected to be the turbulent phenomenon involved in this noise generation mechanism.

Acknowledgments

The authors gratefully acknowledge the Institut du Développement et des Ressources en Informatique Scientifique (IDRIS - CNRS) for providing computing time and for its technical assistance.

References

- ¹Tam, C.K.W., "Jet noise: since 1952," *Theoret. Comput. Fluid Dynamics*, Vol. 10, 1998, pp. 393-405.
- ²Chu, W.T. and Kaplan, R.E., "Use of a spherical concave reflector for jet-noise-source distribution diagnosis," *J. Acoust. Soc. Am.*, Vol. 59, No. 6, 1976, pp. 1268-1277.
- ³Lush, P.A., "Measurements of subsonic jet noise and comparison with theory," *J. Fluid Mech.*, Vol. 46, No. 3, 1971, pp. 477-500.
- ⁴Goldstein, M.E., "Aeroacoustics of turbulent shear flows," *Ann. Rev. Fluid Mech.*, Vol. 16, 1984, pp. 263-285.
- ⁵Mollo-Christensen, E., Kolpin, M.A., and Martuccelli, J.R., "Experiments on jet flows and jet noise far-field spectra and directivity patterns," *J. Fluid Mech.*, Vol. 18, 1964, pp. 285-301.
- ⁶Tam, C.K.W., Golebiowski, M., and Seiner, J.M., "On the two components of turbulent mixing noise from supersonic jets," AIAA Paper 96-1716, May 1996.
- ⁷Viswanathan, K., "Analysis of the two similarity components of turbulent mixing noise," *AIAA Journal*, Vol. 40, No. 9, 2002, pp. 1735-1744.
- ⁸Stromberg, J.L., McLaughlin, D.K., and Troutt, T.R., "Flow field and acoustic properties of a Mach number 0.9 jet at a low Reynolds number," *J. Sound Vib.*, Vol. 72, No. 2, 1980, pp. 159-176.
- ⁹Crighton, D.G., "Acoustics as a branch of fluid mechanics," *J. Fluid Mech.*, Vol. 106, 1981, pp. 261-298.
- ¹⁰Bogey, C. and Bailly, C., "Investigation of subsonic jet noise using LES: Mach and Reynolds number effects," AIAA paper 2004-3023, May 2004.
- ¹¹Zaman, K.B.M.Q., "Flow field and near and far sound field of a subsonic jet," *J. Sound Vib.*, Vol. 106, No. 1, 1986, pp. 1-16.
- ¹²Ukeiley, L.S. and Ponton, M.K., "On the near field pressure of a transonic axisymmetric jet," *Int. J. of Aeroacoustics*, Vol. 3, No. 1, 2004, pp. 43-66.
- ¹³Hileman, J. and Samimy, M., "Turbulence structures and the acoustic far field of a Mach 1.3 jet," *AIAA Journal*, Vol. 39, No. 9, 2001, pp. 1716-1727.
- ¹⁴Bogey, C., Bailly, C., and Juvé, D., "Noise investigation of a high subsonic, moderate Reynolds number jet using a compressible LES," *Theoret. Comput. Fluid Dynamics*, Vol. 16, No. 4, 2003, pp. 273-297.
- ¹⁵Siddon, T.E. and Rackl, R., "Cross-correlation analysis of flow noise with fluid dilatation as source fluctuation," *82nd Meeting of the Acoustical Society of America*, Denver, Oct. 1971.
- ¹⁶Hurdle, P.M., Meecham, W.C., and Hodder, B.K., "Investigation of the aerodynamic noise generating region of a jet engine by means of the simple source fluid dilatation model," *J. Acoust. Soc. Am.*, Vol. 56, No. 6, 1974, pp. 1708-1721.
- ¹⁷Lee, H.K. and Ribner, H.S., "Direct correlation of noise and flow of a jet," *J. Acoust. Soc. Am.*, Vol. 52, No. 5, 1972, pp. 1280-1290.
- ¹⁸Seiner, J.M., "The distribution of jet source strength intensity by means of direct correlation technique," Ph.D. Thesis, Pennsylvania State University, Aug. 1974.
- ¹⁹Dahan, C., Elias, G., Maulard, J., and Perulli, M., "Coherent structures in the mixing zone of a subsonic hot free jet," *J. Sound Vib.*, Vol. 59, No. 3, 1978, pp. 313-333.
- ²⁰Juvé, D., Sunyach, M., and Comte-Bellot, G., "Intermittency of the noise emission in subsonic cold jets," *J. Sound Vib.*, Vol. 71, No. 3, 1980, pp. 319-332.
- ²¹Richardz, W.G., "Direct correlation of noise and flow of a jet using laser Doppler," *AIAA Journal*, Vol. 18, No. 7, 1980, pp. 759-765.
- ²²Schaffar, M., "Direct measurements of the correlation between axial in-jet velocity fluctuations and far field noise near the axis of a cold jet," *J. Sound Vib.*, Vol. 64, No. 1, 1979, pp. 73-83.
- ²³Panda, J. and Seasholtz, R.G., "Experimental investigation of density fluctuations in high-speed jets and correlation with generated noise," *J. Fluid Mech.*, Vol. 450, 2002, pp. 97-130.
- ²⁴Panda, J., Seasholtz, R.G., and Elam, K.A., "Further progress in noise source identification in high-speed jets via causality principle," AIAA paper 2003-3126, May 2003.
- ²⁵Bogey, C., and Bailly, C., "A family of low dispersive and low dissipative explicit schemes for flow and noise computations," *J. Comput. Phys.*, Vol. 194, No. 1, 2004, pp. 194-214.
- ²⁶Bogey, C. and Bailly, C., "Computation of a high Reynolds number jet and its radiated noise using LES based on explicit filtering," To appear in *Computers and Fluids*, 2005.
- ²⁷Rizzetta, D.P., Visbal, M.R., and Blaisdell, G.A., "A time-implicit high-order compact differencing and filtering scheme for large-eddy simulation," *Int. J. Num. Meth. Fluids*, Vol. 42, No. 6, 2003, pp. 665-693.
- ²⁸Bogey, C. and Bailly, C., "Effects of inflow conditions and forcing on a Mach 0.9 jet and its radiated noise," *AIAA Journal*, Vol. 43, No. 5, 2005, pp. 1000-1007.
- ²⁹Bogey, C. and Bailly, C., "Decrease of the effective Reynolds number with eddy-viscosity subgrid-scale modeling," *AIAA Journal*, Vol. 43, No. 2, 2005, pp. 437-439.
- ³⁰Bogey, C., and Bailly, C., "Three-dimensional non reflective boundary conditions for acoustic simulations: far-field formulation and validation test cases," *Acta Acustica*, Vol. 88, No. 4, 2002, pp. 463-471.
- ³¹Zaman, K.B.M.Q., "Far-field noise of a subsonic jet under controlled excitation," *J. Fluid Mech.*, Vol. 152, 1985, pp. 83-111.
- ³²Sabot, J. and Comte-Bellot, G., "Intermittency of coherent structures in the core region of fully developed turbulent pipe flow," *J. Fluid Mech.*, Vol. 74, No. 4, 1976, pp. 767-796.
- ³³Chevray, R. and Tutu, N.K., "Intermittency and preferential transport of heat in a round jet," *J. Fluid Mech.*, Vol. 88, No. 1, 1978, pp. 133-160.